Southern California Earthquake Center (SCEC 3) Final Report

Zhigang Peng (PI)
School of Earth and Atmospheric Sciences
Georgia Institute of Technology, Atlanta, GA, 30338
February 28, 2012

I. Highlight of major research findings in SCEC3

Funding from SCEC3 has supported several lines of research at Georgia Tech's earthquake seismology group over the past few years. The major research findings are summarized below, and some are further elaborated in the technical report submitted together in this report.

1. Dynamic triggering of deep tremor and shallow earthquakes in California

Our project focused on understanding the physical mechanisms and necessary conditions for dynamic triggering of deep tremor and shallow earthquakes in California. Peng et al. [2010] examined triggered earthquakes in the Coso geothermal regions and triggered tremor around Parkfield-Cholame following the 2010 Mw8.8 Chile earthquake. They found that both triggered earthquakes and tremor were consistent with frictional failure at different depths on critically-stressed faults under the Coulomb failure criteria. Peng et al. [2011] found the first evidence of dynamic triggering of microearthquakes at Coso by multiple surface waves of the Chile earthquake. Aiken et al. [in prep, 2012] systematically analyzed triggered microearthquakes in three geothermal regions (Long Valley, Coso and Geysers) in California and found different triggering behaviors. Such differences likely reflect different background seismicity levels or ambient physical conditions in these regions. Chao et al. [2012] found that tremor in the San Jacinto Fault in Southern California (SC) and the Calaveras Fault in Northern California (SC) was not easily triggered by teleseismic earthquakes, when compared with the Parkfield-Cholame section of the San Andreas Fault in Central California (CC). The lack of widespread triggered tremor in NC and SC is not simply a consequence of their different background noise levels from CC, but rather reflects different background tremor rates in these regions.

Peng et al. [2011] found that artificial high-frequency signals could be generated from the analysis procedure when computing spectrograms. They recommended several ways to mitigate such problems. Peng et al. [2012] and Kilb et al. [2012] also converted seismic data into sounds and animations to help convey information about dynamic triggering of tremor and microearthquakes to general audience.

2. Temporal changes of site response and high-frequency bursts during strong motions

In this direction, we conducted a sequence of studies to understand temporal changes of site response induced by strong ground motions. Wu et al. [2010] used sliding window spectral ratio technique to track temporal changes of site response induced by weak to moderate strong ground motions recorded by the borehole seismic network KiK-Net in Japan. They found evidence of nonlinear site response with near instantaneous recovery with peak ground accelerations (PGA) as small as ~20-30 gal. When the PGA is larger than ~60 gal, they observed considerably stronger drops of the peak frequencies followed by logarithmic recovery with time. This may reflect the generation (and then recovery) of additional rock damage. Wu and Peng [2012] applied the same technique to the data recorded by the KiK-Net during the Mw9.1 Tohoku-Oki earthquake. They found evidence of up to 70% co-seismic temporal changes in site response, and followed by two stage of recovery process. The first stage is a rapid recovery within several hours, and the second stage is a slow recovery of more than five months.

We have examined high-frequency (>20 Hz) bursts during the 2004 Mw6.0 Parkfield earthquakes recorded by the dense UPSAR array. Because these bursts were not coherent among nearby stations, we suggested that they were caused by secondary sources immediately beneath each station. Together with Professor Dominic Assamaki in the CEE at Georgia Tech, we are in the process of analyzing and understanding the physical mechanism the high-frequency (>20 Hz) bursts associated with the 3g acceleration recorded at station MYG004 during the Tohoku-Oki mainshock [Peng et al. 2012].

3. Testing static vs. dynamic triggering of aftershocks in southern California

Understanding how earthquakes are triggered by static or dynamic stress changes remains to be one of the most debated topics in earthquake science. We took advantage of the dense seismic observations in SC following the 2010 Mw7.2 El Mayor-Cucapah earthquake, and apply a waveform-based template detection technique to identify missing earthquakes in the Salton Sea geothermal region after the mainshock. Using GPU parallel computing, we have successfully detected ~70 times more earthquakes than listed in the SCSN catalog around the mainshock [Meng et al., 2012]. These newly detected events suggest that dynamic triggering is mostly dominant immediately after the mainshock. However, static triggering became more important in the next few months after the mainshock. We are in the process of applying the same procedure to a larger space-time region in Southern California.

II. 2011 Southern California Earthquake Center Annual Report
Testing static vs dynamic triggering in southern California after the 2010 M7.2 El Mayor-Cucapah Earthquake

Summary

Understanding how earthquakes are triggered by static or dynamic stress changes remains to be one of the most debated topics in earthquake science these days. We took advantage of the dense seismic observations in Southern California following the 2010 magnitude 7.2 El Mayor-Cucapah earthquake, and use them to test the hypothesis of static and dynamic triggering in the Salton Sea geothermal regions. Our past year's effort mainly focused on the following two directions: (1) detecting missing triggered earthquakes in Salton Sea geothermal regions following the El Mayor-Cucapah earthquake based on a waveform matched filter technique; (2) detecting temporal changes of seismic velocities from ambient-noise cross-correlations.

1. Introduction

Large shallow earthquakes are typically followed by increased seismic activities around the mainshock rupture, which are termed "aftershocks". It is well known that aftershock rate generally diminishes with the inverse of the elapsed time since the mainshock following the Omori's law [Omori, 1894; Utsu et al., 1995]. However, the underlying physical mechanism responsible for such temporal decay is still not clear [e.g., Kanamori and Brodsky, 2004]. Recent studies also show that large earthquakes could trigger microearthquakes and tremor at several hundred to thousands of kilometers away [e.g., Hill and Prejean, 2007; Peng and Gomberg, 2010]. While such long-range triggering is mostly due the dynamic stresses from the passing seismic waves, the spatio-temporal behavior and the primary cause of aftershocks (i.e., within 1-2 rupture lengths) and triggered seismicity at intermediate distance (i.e., outside the traditional aftershock zone but within 2-4 rupture lengths) are still not well understood. In particular, whether static or dynamic triggering is the dominant mechanism for triggering seismicity in the near and intermediate distance is currently under heated debate [e.g., Felzer and Brodsky, 2006; Richards-Dinger et al., 2010]. Central to this debate is whether 'stress shadow', or reduction of seismicity at places with negative Coulomb stress changes, does exist or not. Several studies have shown that 'stress shadow' is hard to observe, if not existed at all [Felzer and Brodsky, 2005; Marsan, 2006]. An improved knowledge of the underlying physical mechanism of triggered earthquakes is not only vital for better understanding the fundamental physics of earthquake interaction [e.g., Stein, 1999; Hill and Prejean, 2007], but also useful for seismic hazard forecasting and mitigation [Reasenberg and Jones, 1989; Gerstenberger et al., 2005].

A potential difficulty in studying seismicity rate changes immediately after a large earthquake is that existing earthquake catalogs are not complete, mostly due to masking from the coda waves from the mainshock and large aftershocks [Peng et al., 2006, 2007; Enescu et al., 2007, 2009]. Hence, if we only use events listed in the catalogs to study seismicity rate changes, we may obtain erroneous results. To rule out those potential contaminations caused by missing earthquakes, a systematic examination of continuous waveforms is needed. Recently, Peng and Zhao [2009] applied a waveform matched filter technique and identified about 11 times more aftershocks than listed in the NCSN catalog in the first 2 days after the 2004 Parkfield earthquake. Similarly, Meng et al. [2012b] used the same template events and detected ~10 times more earthquakes than in the NCSN catalog in three days around the San Simeon mainshock. The newly detected events mostly located around the Parkfield section of the San Andreas Fault (SAF), suggesting that Parkfield was positively loaded by the San Simeon earthquake.

We have applied the same technique to detect missing triggered earthquakes around the Salton Sea and the San Jacinto Fault (SJF) following the 2010 Mw7.2 El Mayor-Cucapah earthquake [Meng et al., 2012a]. This is the largest earthquake occurred around the vicinity of southern California after the 1992 Mw7.3 Landers earthquake. Its aftershock zone spans about 120 km long between the southern end of the Elsinore fault and the northern tip of the Gulf of California. Because it caused significant dynamic and static stress changes in southern California, this event provided an excellent opportunity to test whether static or dynamic stress is the primary agent for triggering aftershocks in the near and intermediate field.

3. Seismicity rate changes from SCSN in both regions

We initially focused on the following two regions in southern California: the SJF and the Salton Sea

Geothermal Field (SSGF). We chose these two regions, mostly because of the following three reasons: intensive background seismicity, dense borehole instrumentation, and large stress changes following the 2010 Mw7.2 El Mayor-Cucapah mainshock. In particular, the SJF experienced a ~0.5 bar (e.g., 0.05 MPa) positive static Coulomb stress changes, and the SSGF received a negative Coulomb stress change of similar amplitude. In addition, the entire southern California has experienced ~3-40 cm/s peak ground velocities from the mainshock [Graves and Aagaard, 2011], which corresponds to ~0.3-4.0 MPa dynamic stress changes.

We first downloaded the local earthquake catalog from the SCEDC around the two study regions since 2008. After zooming in around the El Mayor-Cucapah mainshock time, we found that both regions have clear increase of seismic activity immediately after the mainshock (Figure 1). We also computed a smoothed seismicity rate with a window length of 10 data point [Ziv et al., 2003]. As shown in Figure 1e, the seismicity rate around Salton Sea drops below the pre-mainshock rate and remains low for several months. In comparison, the seismicity rate around the SJF is higher than the pre-mainshock rate for a similar duration, including an Mw5.4 earthquake near the Coyote Creek segment of the SJF on 07/07/2010.

4. Matched filter detection of new events in Salton Sea

We have manually checked the waveforms recorded at the the 6 borehole stations (EN network) near Salton Sea, and found many missing earthquakes in the first few hours after the mainshock. To recover those missing earthquakes, we apply the matched filter technique to the Salton Sea geothermal field. The continuous data is from 03/01/2010 to 06/01/2010, or ~34 days before and 57 days after the El Mayor-Cucapah mainshock, respectively. A total of 2088 events from the relocated catalog of Hauksson et al. [2011] are used as templates.

To reduce computation times, we use GPU computing to accelerate the matched filter technique. GPU computing has recently evolved from a fixed-function graphical device into a highly programmable parallel processor [e.g., Nickolls and Dally, 2010] and has been successfully deployed to accelerate a broad range of scientific applications [e.g., Ye et al., 2010]. By dividing the computation of correlations between templates and continuous waveforms into several routines and processing them in parallel on GPU cards, we can achieve a significant speedup for one Nvidia GPU card compared to sequential CPU code [Meng et al., 2012a].

The procedure follows previous work [Peng and Zhao, 2009] and is briefly described as follows. First, we apply a band-pass filter of 10-40 Hz to continuous data and template events to enhance locally generated seismic signal. Each template event must have at least 12 channels (4 stations) with signal-to-noise ratio larger than 5. The signal and noise amplitude is obtained from a 4-s time window starting from 2 s before S-wave arrival and 6 s before P-wave arrival, respectively.

We compute the correlation coefficient (CC) value for all data point within a 4-s time window between the template and continuous waveforms. The 4-s time window is set to be 1 s before and 3 s after *S*-wave arrival time for two horizontal channels, and 1 s before and 3 s after *P*-wave arrival time for the vertical channel. Then, we shift the CC value back to the origin time of the template event by subtracting *S*- or *P*-wave arrival time. Next, we move forward by one data point and repeat the computation for the entire continuous waveform. After we scan through continuous data for all channels and stations, we stack all correlation traces to obtain the mean CC value. We then compute the median absolute deviation (MAD) for each template, and use 9 times the MAD as a detection threshold. For a normal distribution, the probability of exceeding 9 times the MAD is 6.4×10^{-10}, suggesting that it is very unlikely to be a random detection. We finally combine all detections from all templates and assign the location of the detection to that of the template. For multiple detections in each 2-s window, only the detection with the highest correlation coefficient value is kept. The magnitude of the detected event is computed based on the median value of the maximum amplitude ratios for all channels between the detected and template event. Figure 2 shows a positive detection on 04 April 2010 at 22:52:56, approximately 734 s after the El Mayor-Cucapah earthquake. This detection has a mean CC value of 0.45, well above the threshold of 0.14.

So far we have detected a total of ~24000 earthquakes, ~70 times more than listed in the SCSN catalog (Figure 3a-b). Among these events, 4842 earthquakes were before the El Mayor-Cucapah earthquake. We then calculate the seismicity rate changes based on newly detected events and SCSN catalog separately (Figure 6c-d). Despite the large difference in total number of earthquakes, the daily seismicity rate from the newly detected events shows a similar pattern with the SCSN catalog: a significant increase in the first day after the mainshock, and followed by a rapid decrease in the following days, except on the 18th day after the mainshock, when one burst of seismic activity occurred. The seismicity rate dropped below the pre-shock level at about 50 days after the mainshock.

The preliminary results suggest that the matched filter technique is capable of discovering missing locally

triggered earthquakes after the El Mayor-Cucapah earthquake near the Salton Sea. In addition, the seismicity rate changes are roughly consistent with a dynamic stress change (always) immediately after the mainshock, and a long-term negative static stress changes at later time. Our next step is to extend the detection to longer space-time windows in Southern California. Our goal is to obtain a much more complete local catalog, from which we can compute the accurate temporal changes of triggered seismicity rates.

5. Temporal changes of seismic velocity from ambient noise cross-correlations

In addition to examining temporal changes of seismic rates, we also applied a recently developed ambient noise cross-correlation techniques to measure potential changes of seismicity velocity near the SSGF around the 2010 mainshock. The analysis procedure generally follows that of Zhao et al. [2010] and is briefly described as below. Here, we use the daily-long continuous seismic signals recorded at vertical channel (EHZ) in the EN network. The analyzed time window is 35 days before and 60 days after the El Mayor-Cucapah earthquake. To extract the ambient noise signals, we apply a 0.4-1.3 Hz band-pass filter to the data, which is the same as used by Zhao et al. [2010]. Next, we clip the data to reduce the effects of the mainshock and its large aftershocks. We then compute the cross-correlation between all 15 station pairs in frequency domain to obtain the daily empirical Green's function (EGF). For each station pair, all daily EGFs before the mainshock are stacked to obtain the reference trace. Finally, we perform a grid search of the velocity changes by finding the highest CC value between the reference and stretched/compressed daily traces, also known as the stretch/compression method [Wegler et al., 2009].

Figure 4 shows the daily median velocity change 60 days before and after the mainshock. Prior to the mainshock, the seismic velocity changes fluctuated around zero. Immediately after the mainshock, the co-seismic reduction of seismic velocity is up to ~0.3% and followed by a gradual recovery. It appears that the seismicity velocity has not completely return back to the pre-mainshock level even at 60 days after the mainshock.

The sudden drop of seismic velocity immediately after the mainshock is somewhat expected, as recently found for the 2004 Parkfield and many other earthquakes [Brenguier et al., 2008; Zhao et al., 2010]. It is widely accepted that widespread strong ground motion is the most likely cause for the co-seismic velocity reduction in the shallow crust [Rubinstein and Beroza, 2004; Peng and Ben-Zion, 2006; Zhao et al., 2010]. However, it is not clear whether static stress changes induced by the mainshock also play any rule in controlling the coseismic changes and postseismic recovery. We plan to systematically investigate possible seismic velocity changes in southern California associated with the 2010 mainshock in the proposed study.

6. Student Support and Involvement. This project provided full support for the GT graduate student Xiaofeng Meng, who has become an export in detecting earthquakes in Central and Southern California. This work will become a major component of his thesis. Former graduate student P. Zhao (now postdoc at NORSAR) is also partially involved in this project.

7. Reference:

Aiken, C., Z. Peng, and C. Wu (2011), Dynamic triggering of microearthquakes at three geothermal regions in California, *Seismo. Res. Lett.*, 82, 290.

Beroza, G. C. and S. Ide (2011), Slow earthquakes and Nonvolcanic Tremor, *Annu. Rev. Earth Planet. Sci., 39*, 271-296, doi:10.1146/annurev-earth-040809-152531.

Brenguier, F., M. Campillo, C. Hadziioannou, N. M. Shapiro, R. M. Nadeau and E. Larose (2008), Postseismic relaxation along the San Andreas fault at Parkfield from continuous seismological observations, *Science*, 321, 1478–1481.

Chao, K., Z. Peng, C. Wu, C.-C. Tang, and C.-H. Lin (2012), Remote triggering of non-volcanic tremor around Taiwan, *Geophys. J. Int.*, 188, 301-324, doi: 10.1111/j.1365-246X.2011.05261.x.

Chao, K., Z. Peng, A. Fabian, and L. Ojha (2012), Comparisons of triggered tremor in California, *Bull. Seismol. Soc. Am.*, 102(2), doi: 10.1785/0120110151.

Doran, A., X. Meng, Z. Peng, C. Wu and D. Kilb (2010), Dynamic triggering of earthquakes in the Salton Sea region of Southern California from large regional and teleseismic earthquakes, *Eos Trans. AGU*, *91*, Fall Meet. Suppl., Abstract S33B-2104.

Enescu, B., Mori, J. and M. Miyazawa (2007), Quantifying early aftershock activity of the 2004 mid-Niigata

Prefecture earthquake (Mw6.6), *J. Geophys. Res.*, 112, B04310, doi:10.1029/2006JB004629.
Enescu, B., J. Mori, M. Miyazawa, and Y. Kano (2009), Omori-Utsu law c-values associated with recent moderate earthquakes in Japan, *Bull. Seismol. Soc. Am.*, 99(2A), 884-891, doi: 10.1785/0120080211.
Felzer, K. R., and E. E. Brodsky (2005), Testing the stress shadow hypothesis, *J. Geophys. Res.,* 110, B05S09, doi:1029/2004JB003277.
Felzer, K., and E. Brodsky (2006), Decay of aftershock density with distance indicates triggering by dynamic stress, *Nature,* 441, 735-738.
Gerstenberger, M. C., S. Wiemer, L. M. Jones, and P. A. Reasenberg (2005), Real-time forecasts of tomorrow's earthquakes in California, *Nature*, *435*, 328–331, doi:10.1038/nature03622.
Graves, R. W. and B. T. Aagaard (2011), Testing long-period ground-motion simulations of scenario earthquakes using the Mw 7.2 El Mayor-Cucapah mainshock, *Bull Seism Soc Am.*, 101(2), 895-907; doi: 10.1785/0120100233.
Hauksson, E. and W. Yang, and P. M. Shearer (2012), Waveform Relocated Earthquake Catalog for Southern California (1981 to 2011), Submitted to *Bull. Seismol. Soc. Am.*
Hill, D. P., and S. G. Prejean (2007), Dynamic triggering, in Treatise on Geophysics, 257–292, ed. Schubert, G., Vol. 4: Earthquake Seismology, ed. Kanamori, H., Elsevier, Amsterdam.
Kanamori, H and E. E. Brodsky (2004), The physics of earthquakes, *Rep. Prog. Phys.,* 67, 1429 doi:10.1088/0034-4885/67/8/R03.
Kilb, D., Z. Peng, D. Simpson, A. Michael, M. Fisher and D. Rohrlick (2012), Listen, watch, learn: SeisSound video products, *Seismol. Res. Lett.*, 83(2), 281-286, doi: 10.1785/gssrl.83.2.281.
Marsan, D. (2006), Can coseismic stress variability suppress seismicity shadows? Insights from a rate-and-state friction model, *J. Geophys. Res.,* 111, B06305, doi:10.1029/2005JB004060.
Meng, X., X. Yu, Z. Peng and B. Hong (2012a), Detecting earthquakes around Salton Sea following the 2010 M_w7.2 El Mayor-Cucapah earthquake using GPU parallel computing, *Procedia Computer Science*, submitted
Meng, X., Z. Peng, and J. L. Hardebeck (2012b), Detecting missing earthquakes on the Parkfield section of the San Andreas Fault following the 2003 *Mw*6.5 San Simeon earthquake, *Geophys. Res. Lett.*, in prep.
Meng, X., Z. Peng and P. Zhao (2011), Differentiating dynamic versus static triggering following the 2010 *Mw*7.2 El Mayor-Cucapah earthquake, AGU 2011 Fall meet. Abstract S21D-02.
Nickolls, J. and W. J. Dally (2010). The GPU Computing Era, IEEE Micro 30(2), 56-69.
Omori, F. (1894), On the aftershocks of earthquakes, *J. Coll. Sci. Imp. Univ. Tokyo*, *7*, 111–200.
Peng, Z., and Y. Ben-Zion (2006), Temporal changes of shallow seismic velocity around the Karadere-Duzce branch of the north Anatolian fault and strong ground motion, *Pure Appl. Geophys.*, 163, 567-599, doi: 10.1007/s00024-005-0034-6.
Peng, Z., and P. Zhao (2009), Migration of early aftershocks following the 2004 Parkfield earthquake, *Nature Geosci.,* 2, 877–881, doi: 10.1038/ngeo697.
Peng, Z., and J. Gomberg (2010), An integrated perspective of the continuum between earthquakes and slow-slip phenomena, *Nature Geosciences*, v. 3, p. 599-607, doi:10.1038/ngeo940.
Peng, Z., J. E. Vidale, and H. Houston (2006), Anomalous early aftershock decay rates of the 2004 M6 Parkfield earthquake, *Geophys. Res. Lett.*, 33, L17307, doi:10.1029/2006GL026744.
Peng, Z., J. E. Vidale, M. Ishii, and A. Helmstetter (2007), Seismicity rate immediately before and after main shock rupture from high-frequency waveforms in Japan, *J. Geophys. Res.*, 112, B03306, doi:10.1029/2006JB004386.
Peng, Z., D. P. Hill, D. R. Shelly, and C. Aiken (2010), Remotely triggered microearthquakes and tremor in Central California following the 2010 Mw8.8 Chile Earthquake, *Geophys. Res. Lett.*, *37*, L24312, doi:10.1029/2010GL045462.
Peng, Z., C. Wu, and C. Aiken (2011a), Delayed triggering of microearthquakes by multiple surface waves circling the Earth, *Geophys. Res. Lett.*, *38*, L04306, doi:10.1029/2010GL046373.
Peng, Z., L. T. Long, and P. Zhao (2011), The relevance of high-frequency analysis artifacts to remote triggering, *Seismol. Res. Lett.*, 82(5), 654-660, doi: 10.1785/gssrl.82.5.654.
Peng, Z., C. Aiken, D. Kilb, D. Shelly, B. Enescu (2012), Listening to the 2011 magnitude 9.0 Tohoku-Oki, Japan earthquake, *Seismol. Res. Lett.*, 83(2), 287-293, doi: 10.1785/gssrl.83.2.287.
Reasenberg, P. A., and L. M. Jones (1989), Earthquake hazard after a mainshock in California, *Science*, *243*, 1173–1176.

Richards-Dinger, K., R. Stein, and S. Toda (2010), Decay of aftershock density with distance does not indicate triggering by dynamic stress. *Nature*, *467*(7315), 583-586.

Stein, R. S. (1999), The role of stress transfer in earthquake occurrence, *Nature*, 402, 605-609.

Utsu, T., Y. Ogata, and R. S. Matsu'ura (1995), The centenary of the Omori formula for a decay law of aftershock activity, *J. Phys. Earth*, *43*(1), 1–33.

Wegler, U., H. Nakahara, C. Sens-Schönfelder, M. Korn, and K. Shiomi (2009), Sudden drop of seismic velocity after the 2004 Mw 6.6 Mid-Niigata earthquake, Japan, observed with Passive Image Interferometry, *J. Geophys. Res.,* v. 114, B06305, doi:10.1029/2008JB005869.

Wu, C., Z. Peng, and Y. Ben-Zion (2010), Refined thresholds for nonlinear ground motion and temporal changes of site response associated with medium size earthquakes, *Geophys. J. Int.*, 183, 1567-1576, doi: 10.1111/j.1365-246X.2010.04704.x.

Wu, C., and Z. Peng (2011), Temporal changes of site response during the M9.0 off the Pacific coast of Tohoku earthquake, *Earth Planets Space*, 63(7), 791-795, doi:10.5047/eps.2011.06.011.

Wu, C., and Z. Peng (2012), Long-term change of site response after the Mw9.0 Tohoku earthquake in Japan, *Earth Planets Space*, in revision.

Wu, C., Z. Peng and D. Assimaki (2012), Long-term change of site response and high-frequency radiations associated with the Mw9.0 Tohoku-Oki Earthquake in Japan, submitted to the Annual Seismological Society of America meeting, San Diego, April 2012.

Ye, X., D. Fan, et al. (2010), High performance comparison-based sorting algorithm on many-core GPUs, Proc. IEEE Int Parallel & Distributed Processing (IPDPS) Symp: 1-10.

Zhao, P., Z. Peng, and K. Sabra (2010), Detecting remotely triggered temporal changes around the Parkfield section of the San Andreas Fault, *Earthquake Science*, Special Issue on Ambient Noise Seismology, doi: 10.1007/s11589-010-0748-0.

Ziv, A., A. M. Rubin, and D. Kilb (2003), Spatiotemporal analyses of earthquake productivity and size distribution; observations and simulations, *Bull. Seismol. Soc. Am* **93**, 2069–2081.

III. Figures that highlight your research with captions

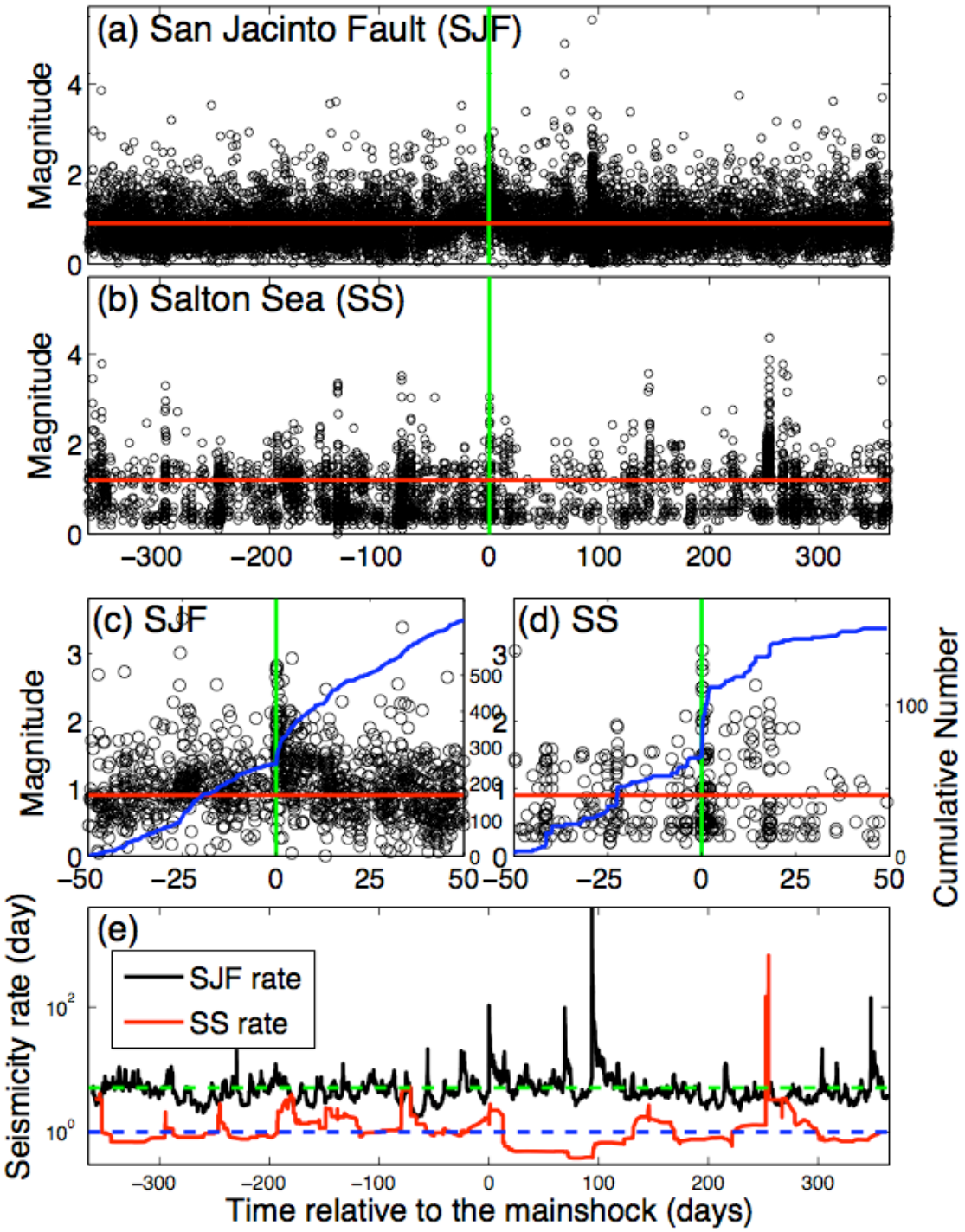

Figure 1. (a) Magnitudes versus times relative to the mainshock for all earthquakes around the San Jacinto Fault (SJF) since 2005. The solid red lines mark the magnitude of completeness Mc value. (b) Magnitudes versus time for all earthquakes around the Salton Sea (SS). (c-d) A zoom-in plot of the seismicity around the SJF and the SS within 30 days of the mainshock. The blue line shows the cumulative number above the Mc value. (e) The smooth seismicity rates with relative times for the SJF (black) and SS (red).

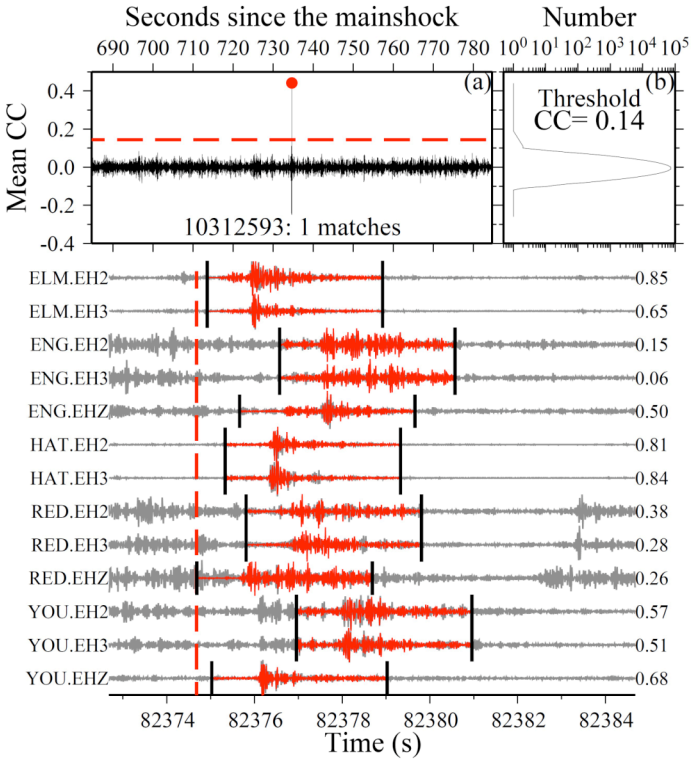

Figure 2. An example of newly detected event near Salton Sea after the El Mayor-Cucapah mainshock. (a) Mean correlation coefficient trace versus time for the template event 10379125. The red dot corresponds to the detected event at ~12 min after the mainshock; (b) The histogram of the mean CC function; (c) A comparison of the template waveforms (red) and the continuous waveforms (grey) around the origin time of detected event (vertical dashed line). The channel names and the corresponding CC values are labeled on the left and right sides, respectively.

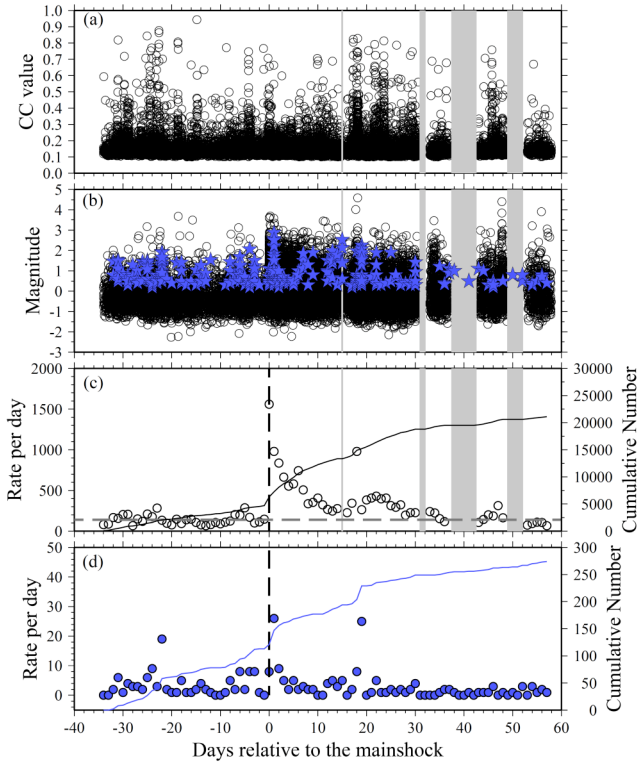

Figure 3. Summary of newly detected events and the SCSN catalog. (a) The CC values versus the origin times of all detected events. The gray shadow areas mark the gap in the continuous data. (b) The magnitudes versus the origin times of all detected events (black circles) and earthquakes listed in the SCSN catalog (blue stars), respectively. (c) Seismicity rate of all detected events in the Salton Sea geothermal field. (d) Seismicity rate of earthquakes listed in the SCSN catalog. Other notations are the same with that of (c).

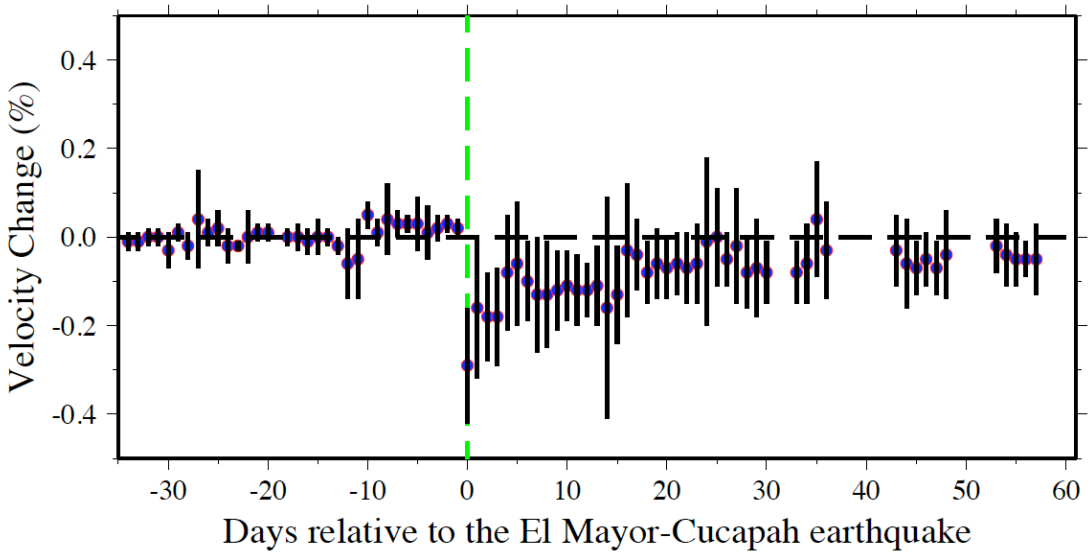

Figure 4. Median daily velocity changes in Salton Sea from all possible station pairs versus days relative to the mainshock (the vertical green dashed line). The vertical short black lines represent the median absolute deviations (MAD) of measurement for each day.

IV. Information on outreach activity you have performed during SCEC3

The PI Peng has given multiple seminars and talks on the findings of non-volcanic tremor in Central and southern California at various institutions during SCEC3. These include the USGS Menlo Park (Summer, 2010), China Earthquake Administration in 2008 and 2011, and Caltech Seismolab in Spring 2009.

In addition, PI Peng has hosted a total of 5 SCEC summer interns during SCEC 3 (Summer Ohlendorf, Summer 2007; Amanda Fabian and Lujendra Ojha, Summer 2009; Adrian Doran and Meghan Fisher, summer, 2010). They have been working on various projects that are directly or partially funded by SCEC3. Their work has been presented at previous SCEC, AGU and SSA annual meetings, and some have resulted in peer-review publications [e.g., Chao et al., 2012; Kilb et al., 2012].

V. A bibliography of all publications supported by SCEC3 funds including papers in review (by calendar year)

Fischer, A., Z. Peng, and C. G. Sammis (2008), Dynamic triggering of high-frequency bursts by strong motions during the 2004 Parkfield earthquake sequence, *Geophys. Res. Lett.*, 35, L12305, doi:10.1029/2008GL033905.

Wu, C., Z. Peng and Y. Ben-Zion (2009a), Non-linearity and temporal changes of fault zone site response associated with strong ground motion, *Geophys. J. Int.*, 176, 265-278, doi: 10.1111/j.1365-246X.2008.04005.x.

Wu, C., Z. Peng, and D. Assimaki (2009b), Temporal changes in site response associated with strong ground motion of 2004 Mw6.6 Mid-Niigata earthquake sequences in Japan, *Bull. Seismol. Soc. Am.*, 99(6), 3487–3495, doi: 10.1785/0120090108.

Wu, C., Z. Peng, and Y. Ben-Zion (2010), Refined thresholds for nonlinear ground motion and temporal changes of site response associated with medium size earthquakes, *Geophys. J. Int.*, 183, 1567-1576, doi: 10.1111/j.1365-246X.2010.04704.x.

Peng, Z., D. P. Hill, D. R. Shelly and C. Aiken (2010), Remotely triggered microearthquakes and tremor in Central California following the 2010 Mw8.8 Chile Earthquake, *Geophys. Res. Lett.*, 37, L24312, doi:10.1029/2010GL045462.

Peng, Z., C. Wu, and C. Aiken (2011), Delayed triggering of microearthquakes by multiple surface waves circling the Earth, *Geophys. Res. Lett.*, *Geophys. Res. Lett.*, 38, L04306, doi: 10.1029/2010GL046373.

Shelly, D. R., Z. Peng, D. P. Hill and C. Aiken (2011), Triggered creep as a possible mechanism for delayed dynamic triggering of tremor and earthquakes, *Nature Geosci.*, 4, 384–388, doi: 10.1038/ngeo1141.

Peng, Z., L. T. Long, and P. Zhao (2011), The relevance of high-frequency analysis artifacts to remote triggering, *Seismol. Res. Lett.*, 82(5), 654-660, doi: 10.1785/gssrl.82.5.654.

Wu, C., and Z. Peng (2011), Temporal changes of site response during the M9.0 off the Pacific coast of Tohoku earthquake, *Earth Planets Space*, 63(7), 791-795, doi:10.5047/eps.2011.06.011.

Chao, K., Z. Peng, A. Fabian, and L. Ojha (2012), Comparisons of triggered tremor in California, *Bull. Seismol. Soc. Am.*, 102(2), doi: 10.1785/0120110151.

Wu, C., and Z. Peng (2012), Long-term change of site response after the Mw9.0 Tohoku earthquake in Japan, *Earth Planets Space*, in revision.

Kilb, D., Z. Peng, D. Simpson, A. Michael, M. Fisher and D. Rohrlick (2012), Listen, watch, learn: SeisSound video products, *Seismol. Res. Lett.*, 83(2), 281-286, doi: 10.1785/gssrl.83.2.281.

Peng, Z., C. Aiken, D. Kilb, D. Shelly, B. Enescu (2012), Listening to the 2011 magnitude 9.0 Tohoku-Oki, Japan earthquake, *Seismol. Res. Lett.*, 83(2), 287-293, doi: 10.1785/gssrl.83.2.287.

Meng, X., X. Yu, Z. Peng and B. Hong (2012), Detecting earthquakes around Salton Sea following the 2010 M_w7.2 El Mayor-Cucapah earthquake using GPU parallel computing, *Procedia Computer Science*, submitted.